Effect of Surfactant type on the Characteristics and Bioactivity of Mesoporous Bioactive Glasses

Hediyeh Nejati Rad[1], Aliasghar Behnamghader[1],*, Mojgan Bagheri[1], Masoud Mozafari[2]

[1]Nanotechnology and Advanced Materials Department, Materials and Energy Research Center (MERC), Tehran, Iran
[2]Department of Tissue Engineering & Regenerative Medicine, Faculty of Advanced Technologies in Medicine, Iran University of Medical Sciences, Tehran, Iran

*Corresponding author: E-mail: behnamghader@yahoo.com

In this study, mesoporous bioactive glass 77S was synthesized by sol-gel method using two different ionic and nonionic surfactants. Physical-chemical properties of synthesized Bioglass were studied using techniques include X-ray diffraction, scanning electron microscopy, nitrogen adsorption and Fourier transform infrared spectroscopy. The results showed that using nonionic and ionic surfactants increased specific surface area by 3 and 5 times, respectively. By determining the silicon release in three different temperatures, the activation energy values of Si-O-Si for sample with surface area of 161 and 94 m^2/g were calculated 1/10 and 1/5 of control glass with surface area of 34 m^2/g. The pH of sample was evaluated in solutions buffered with TRIS. pH analysis results suggested a direct relation between surface area and pH changes, the greatest increase in pH was observed in the sample with the highest surface area. Moreover, the in vitro bioactivity test was also conducted in simulated body fluid (SBF) and formation of apatite layer was evaluated by scanning electron microscopy and X-ray diffraction after a day.

Introduction

During the last decades, the bone diseases and trauma have significantly increased. The need of artificial replacement which can be used to repair or reconstruct damaged part has always been the driving force behind the discovery and design of new biomaterial. As a result, using bone graft as a substitute for defective bones has attracted a lot of attention. In some cases, bioactive glasses are available for use due to their ability to attach to bone chemically [1-3]. Bioactive glasses play a fundamental role in bone graft field due to osteoconductive, osteoproductive and osteoinductive properties. Further, high biocompatibility, positive biological effects, as well as bonding and integrating with living bone have made bioactive glasses as one of the most interesting bone graft materials during recent years [4-6]. Bone-bonding ability of bioactive glasses is attributed to the formation and growth of a hydroxyl carbonated apatite (HCA) layer, which its composition is similar to mineral phase of bone. This similarity let bioactive glasses have strong interaction and integration with bone [52]. The hydroxyl carbonated apatite (HCA) layer is formed on the surface of glasses when they are soaked in simulated body fluid (SBF) or implanted in vivo [7]. Further, the mechanism of formation HA layer initiates with exchanging Alkali ions (Na^+ or Ca^{2+}) with H^+ from the solution or body fluids, formation of silanol groups (SiOH), dissolution of the silica glass network and polymerization of silica gel film by poly-condensation of silanol groups. Subsequently an amorphous calcium phosphate layer develops within the silica-rich layer, and the HA layer crystallizes, producing a hydroxycabonate apatite (HCA) layer [8,9,33].

These reactions occur only through a few hours for highly bioactive glasses. Based on the above-mentioned stages, the degradation of ionic products, especially silica, can be considered as a sign of bioactivity of the bioglasses. In summary, the ability of bioactive glasses for formation of HA layer and tissue repair is related to their chemical composition and their textural properties such as porosity, pore volume, pore size, and pore structure, which play a role in releasing ion [11-14]. Mesoporous bioactive glasses (MBG) have attracted great attention due to their large surface area and their property during last 20 years [15]. Further, these materials can act as a drug carrier owing to their outstanding textural properties of mesoporous bioactive glasses [16-18-55].

To prepare MBG, the supramolecular chemistry has been combined into sol-gel process [19]. In this case, structure-directing agents play an important role in producing mesoporous structure. Under synthesis conditions, these molecules are self-organized into micelles, and linked to the hydrophilic part of silica precursors, which results in formation of a self-assembly mesophase [1]. Finally, after drying of the product, the surfactant is removed and a mesoporous structure with high surface area and porosity is obtained.

The present study aimed to investigate the effect of surfactant type on the textural properties and bioactivity of bioactive glass 77S. To this aim, an anionic surfactant, sodium dodecyl sulfate and a nonionic surfactant, Triton X-100 were used to produce the mesoporous structure of glass 77S. Three mesoporous bioactive glass samples 77S (including control sample without surfactant) in the system of SiO_2- P_2O_5 –CaO were synthesized and characterized to

Advanced Materials Letters
www.vbripress.com/aml

IAAM®
Advancement of Materials to Global Excellence
www.iaamonline.com

examine the effects of surfactant type on the specific characteristics of the synthesized samples.

Experimental procedure

Materials

Tetraethyl orthosilicate (Si(OC$_2$H$_5$)$_4$, TEOS) (99% from Aldrich), triethyl phosphate (OP(OC$_2$H$_5$)$_3$, TEP) (99.8% from Aldrich), calcium nitrate tetrahydrate (Ca(NO$_3$)$_2$.4H$_2$O) (Applichem) were used as silicon, phosphorous, and calcium sources. The surfactants sodium dodecyl sulfate (SDS- NaC$_{12}$H$_{25}$SO$_4$) (Merck) and triton X-100 ((C$_{14}$H$_{22}$O(C$_2$H$_4$O)$_n$(n=9-10)) (Merck) were used as structure directing agent. In addition, deionized water and ethanol (from Merck) were used as solvent and 0.1 mol L^{-1} nitric acid (HNO$_3$) were utilized as catalyst.

In order to measure pH variation through soaking, Tris-buffer solutions (pH =5.3, 7.4, 9) were prepared by using hydrochloric acid and Tris (hydroxymethyl) aminomethane (THAM)(Merck).

Synthesis

At the first step, the surfactant was dissolved in deionized water and nitric acid media at room temperature. Then, absolute ethanol, TEOS, TEP and Ca(NO$_3$)$_2$ were added, respectively. After the final addition, the solution was taken under stirring condition for 1 hour in order to complete the hydrolysis process. The solution was kept at 50ºC overnight until the gel was formed and then the gel was dried at 120ºC. Finally, the dried gel was heated at 550ºC for 1.5 hours to eliminate the residual nitrate and organic substances.

The synthesized samples in the presence of SDS and Triton-X100 were coded as BGS glass and BGT glass, respectively. The control sample, BGC, synthesized without using surfactant.

Characterization of bioactive glasses

Thermal behavior: The phase transitions were monitored by using differential thermal analysis (DTA) and thermal gravimetric analysis (TGA) in order to estimate the stabilizing and crystallization temperatures of the glasses. So, BÄHR 503 (Germany) instrument was employed and the glasses were heated up to 1000ºC at a heating rate of 10ºC/min.

Chemical structure and phase characterization: Powder X-ray diffraction (XRD) patterns were recorded using Simens X-ray diffractometer with Cu-Kα radiation and X-ray wavelength of 1.540 Å. Diffractometer operated at 20 kV and 10 mA with the step size of 0.05 over the 2Θ ranged between 10-80°. Further, Fourier transform infrared spectroscopy (FTIR) were performed by using Spectrum RXI (USA). Bioactive glass powders were mixed with KBr powder and pressed into a disk suitable for measuring FTIR. Finally, the FTIR spectra were recorded from 4000 cm^{-1} to 400 cm^{-1}.

Morphology characterization: Field emission scanning electron microscopy (FE-SEM) (Mira3-XMU) on gold-coated specimens was used to examine the morphological and textural features of the bioactive glasses.

N2 adsorption–desorption isotherms, surface area and pore size: The surface area of samples was calculated via the Brunauer-Emmett-Teller (BET) method and the pore size of samples was obtained from the maxima of the pore size distribution curve calculated by the Barrett- Joyner-Halenda (BJH) method by using Belsorp Miniц with nitrogen as an absorbent at 77K.

Ion release and in vitro cellular bioactivity: The ion solubility tests were first conducted at three different temperatures by soaking 100 mg of bioactive glasses in 100 mL of Tris-buffer at pH 7.4. The silicon concentration was analyzed by coupled plasma atomic emission spectroscopy (ICP-OES) Vistra-Pro inductively. The ion solubility tests were carried out at room temperature by soaking of each bioactive glasses in Tris-buffer (pH=5.3, 7.4 and 9). pH of the solutions was measured with pH meter (MA 235 Mettledo-Toledo) during the soaking period.

In vitro bioactivity test for BGS glass was performed by soaking the bulks prepared from BGS powder into simulated body fluid (SBF) at 37℃ under stirring. After 1, 10 and 20 days of soaking, the samples were removed and washed with distilled water.

Results and discussion

Materials characterization

Fig. 1 illustrates the XRD patterns of the samples BGC, BGS and BGT. As shown, no characteristic diffraction was observed in the pattern except for broad band observed at 2θ values in the range of 20–30∘ for the three samples which indicating that all the samples are amorphous. The broad band in the range of 20–30∘ was also found in similar works [**38,39**]. This broad band is suggested to be due to high percentage of amorphous particles in the samples [**40, 41**].
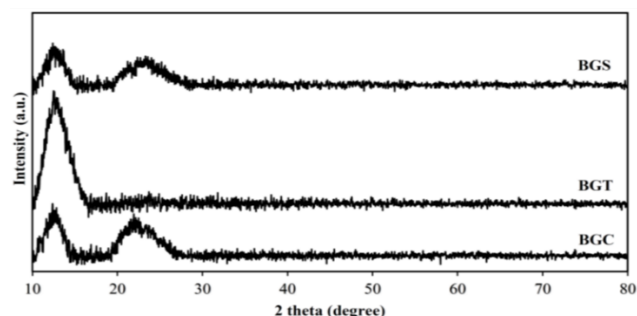

Fig. 1. The XRD pattern of samples BGC, BGT and BGS.

The simultaneous TG/DTA results of all samples are shown in **Fig. 2**. Based on the results, all the samples have similar weight loss regions. Weight loss at the first stage is about 10%, 5% and 15% for the samples BGC, BGT and BGS, respectively, which can be related to the removal of chemically adsorbed water and correlated with an endothermic peak at 100-150ºC in the DTA curve. Regarding BGT glass powder, Triton X-100 can be

**Advanced
Materials Letters**
www.vbripress.com/aml

IAAM®
Advancement of Materials
to Global Excellence

www.iaamonline.com

oxidized by three steps, starting from 300ºC to 500ºC [**26**]. As observed in the TG curve of BGT, the most weight loss appears between 200-500ºC due to the surfactant decomposition. TG results for BGS indicate that the residual weight fails to level off up to 1000ºC, due to the gradual decomposition of SDS surfactant in BGS [**27**]. Another endothermic peak at 500-550ºC observed in sample BGS can be related to alkyl/nitrate groups. Large exothermic peak at 700ºC which is more obvious in sample BGT are related to the crystallization of calcium-silicate phases in Bioglass [**28**].
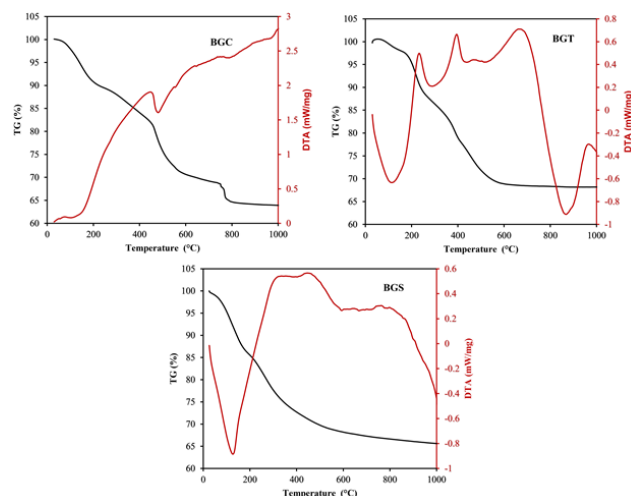
structures [**56**]. Sample BGC indicates an isotherm curve with H2-type hysteresis loop with smoothly increasing adsorption branch followed by a desorption branch step. Based on the hysteresis loop, the shape of pores would be ink bottle with wide bodies and narrow necks [**29,30**]. Further, both samples BGT and BGS show H3 hysteresis loops without any limitation to adsorb nitrogen at high P/P_0. The samples with H3 hysteresis loop might have plate-like particles with slit-shaped pores. A steep region so-called tensile strength at pressure range from 0.4-0.45 is observed in the hysteresis loop [**31**].
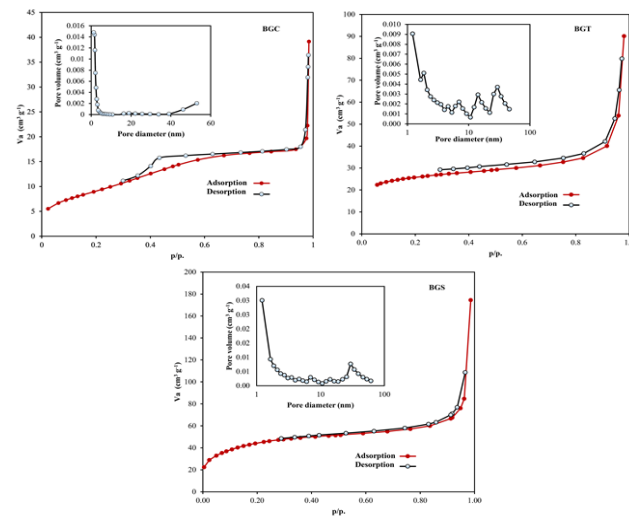

Fig. 2. TG/DTA curves of samples BGC, BGT and BGS.

Fig. 3. N$_2$ adsorption/desorption isotherms of samples BGC, BGT and BGS.

Table 1 displays the textural parameters of BGC, BGT, and BGS. Based on the results, S_{BET} and pore volume increased in both of the samples synthesized with the surfactant due to the formation of mesopore structure after removing the surfactant through heat treatment. A remarkable increase was observed in S_{BET} of BGS in which mesoporous structure is derived from SDS as a structure-directing agent. In fact, the surface area relies on the chemical interaction between silica and surfactants [**29**]. Further, the interaction between ionic head group of surfactant (S) and inorganic precursors (I) is related to the electrostatic repulsion which is a driving force for the self-assembly of silica-micelle [**47,48**]. Isoelectric point (pI) of silica is ~ 2 and silica species are the protonated, at a pH<2 inorganic precursors would have positive charge (I$^+$) and vice versa [**49**]. In case of using anionic surfactant, the possible synthetic rout should be follows as S$^-$I$^+$. Under acidic condition, interaction between positively charged silica oligomers and surfactant would be weak and might lead only lamellar and disordered mesostructured [**50**]. While, the chemical interactions in nonionic surfactants are based on hydrogen bonding due to electrically-neutral strategy and it follow S^{0}I^0 synthetic rout [**42**].

Table 1. Texture properties of the bioactive glasses.

Sample	S_{BET} (m^2/g)	Pore size (nm)	Pore volume (cm^3/g)
BGC	34	7.1	0.03
BGT	94	5.9	0.11
BGS	161	6.7	0.21

Fig. 4 displays the FTIR spectra of BGC, BGT and BGS in the 400-4000 cm^{-1}. The silica vibrations at 456, 796 and 1080 cm^{-1} can be assigned to Si-O-Si bending, Si-O-Si symmetric stretching and Si-O-Si asymmetric stretching modes, respectively [**32,33**]. P-O be nding band of PO$_4$$^{3-}$ group is observed at 606 cm^{-1} and 1260 cm^{-1} more, the band at 1673 cm^{-1} and the small peak at 3740 cm^{-1} can be related to the adsorbed water at the surface of glasses and silanol groups, respectively [**33**]. All the samples indicated similar characteristics of the absorption bands.
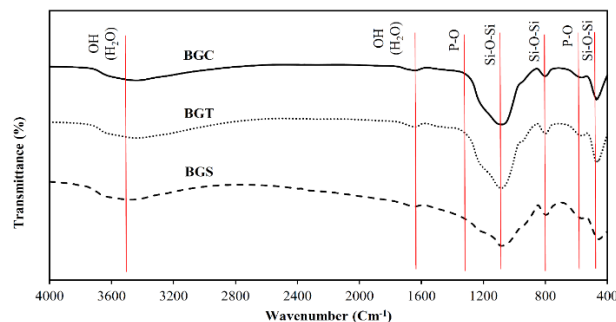
Fig. 3 illustrates the nitrogen adsorption isotherms and pore diameter distribution of samples BGC, BGT and BGS. The isotherm curve for all samples is identified as type IV according to IUPAC classification with Sharp inflections in the P/P_0, which is typically observed in mesoporous

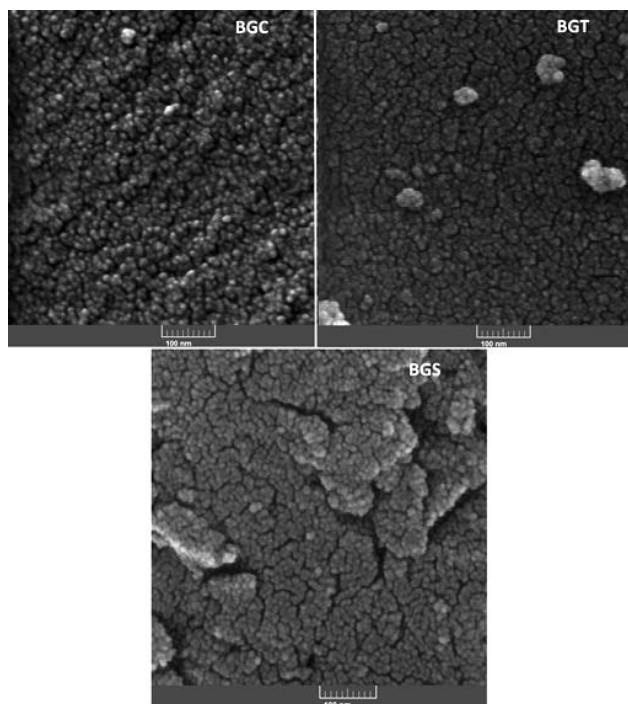**Fig. 4.** The FT IR spectra of samples BGC, BGT and BGS.

Fig. 5. SEM micrographs of samples BGC, BGT and BGS.

The FE-SEM images of sample BGC, BGT and BGS are shown in **Fig. 5**. Based on the results, all of the samples are porous although sample BGS has more porosity, compared to BGC and BGT, which is in agreement with BET results. It is indicated that micelles grow as the same time as the silica walls are built around the micelles so porosity appears when the speed of growing of micelles and building of silica walls are the same [**43**].
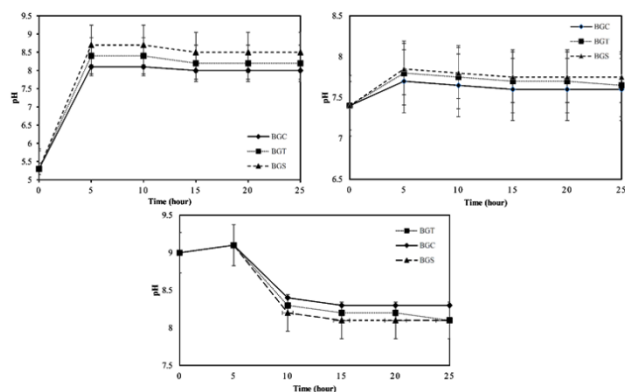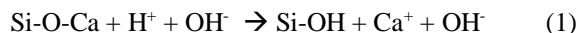

Fig. 6. pH of samples BGC, BGT and BGS dissolution in different condition by the time.

Dissolution tests

Fig. 6 displays the results of dissolution experiment in different conditions (acidic, neutral and basic). As shown, an increase in pH is observed for all samples in the initial period of dissolution due to the exchange between Ca^{2+} and H^{+} ions in solution. According to Hench's theory, the formation of Si-OH from Si-O-NB after releasing Ca^{2+} results in increasing pH as follows [**33**]:

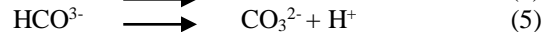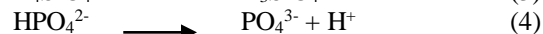$$Si\text{-}O\text{-}Ca + H^{+} + OH^{-} \rightarrow Si\text{-}OH + Ca^{+} + OH^{-} \qquad (1)$$

Then, the second stage of Hench's theory occurs after an increase in pH. The reason for decreasing in pH for all samples can be explained by the hydrolysis of Si-O-Si through the dissolution of $Si(OH)_4$ which is facilitated by increasing the pH in the first stage [34].

$$2(Si\text{-}O\text{-}Si) + 2(OH^{-}) \rightarrow Si\text{-}OH + Si\text{-}OH \qquad (2)$$

Regarding higher surface area of sample BGS, more pH changes has been recorded in that sample in comparison with samples BGC and BGT. In fact, the formation of Si-OH and the silicon release is easier in the glasses with higher surface area. Hence, the glasses with higher surface area tend to show the highest change in pH due to a better interaction between glass and buffer solution. It is suggested by Tabia *et al.* [**44**] that bioactive glasses with higher surface area are more prone to dissolution and have more intense ionic exchange between their surface and the surrounding medium. As a result, a significant increase of the pH is expected in bioactive glasses with high surface area.

In the basic condition, a decrease in pH is observed after 20 hours of reaction because of precipitating carbonates and calcium phosphates. The same result detected by Cerruti *et al.,* [**46**]. At pH >8, the reactions are as follow:

$$H_4SiO_4 \longrightarrow H_3SiO_4^{-} + H^{+} \qquad (3)$$
$$HPO_4^{2-} \longrightarrow PO_4^{3-} + H^{+} \qquad (4)$$
$$HCO^{3-} \longrightarrow CO_3^{2-} + H^{+} \qquad (5)$$

Ló pez-Noriega *et al.,* [**45**] reached the same pattern for pH changes in the similar work.
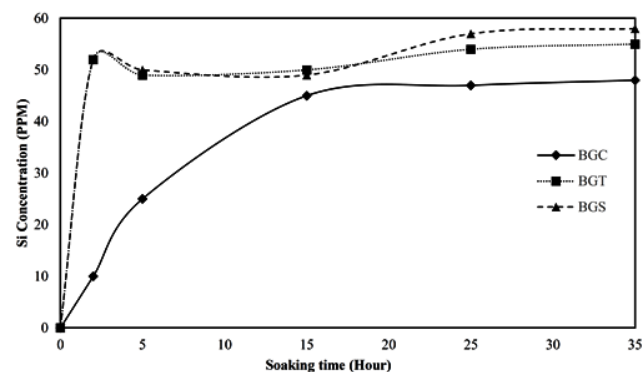

Fig. 7. Silicon release from samples BGC, BGT and BGS after 35 hours soaking in buffer with pH of 7.4.

Fig. 7 demonstrates the amounts of silicon released from the glasses in buffer with pH of 7.4 at room temperature. As shown in **Fig. 7**, the highest release of silicon was observed in the sample BGS glass after 35 h. Moreover, a significant difference was observed during in-vitro experiments among the glasses because of their surface area. The bioactive glasses of BGS and BGT displayed a rapid silicon release during the first 5 h and then followed by a plateau until the end of test. Further, the amount of released silicon from the sample BGC was less

than the treated samples with surfactants (BGS and BGT). These differences in silicon release between treated and non-treated samples can be attributed to their surface areas. In order to calculate activation energy (Ea), the silicon release test was conducted at 20, 35 and 60 °C for a duration of 6 h. The value of activation energy calculated via the following equation (6) as ionic diffusion model [34].

$$Ln[Si] = Ln[SiO] – Ea/KT \qquad (6)$$

The activation energy for BGS glass is equal to 0.05eV, which is lower than two other samples. BGC glass indicates the highest Ea, 0.53 eV, which is ten times higher than BGS (0.05 ev) and Ea sample BGC showed Ea (0.12 ev) between BGC and BGS. Our results are similar to those founded by Acros et al., [51], in which Ea was studied as a parameter to predict bioactivity of glasses.

In vitro behavior analysis

Sample BGS was selected for more in vitro experiments as it involves higher surface area and silicon ion release than other samples. **Fig. 8** illustrates the XRD pattern of sample BGS after soaking in SBF during 20 days. The XRD results indicated that the initial sample BGS has amorphous structure but a crystalline phase was formed gradually after soaking the sample in SBF. Only after a day soaking in SBF, the XRD diagram shows the present of peaks at 25.8° and 31.9° which corresponding to the (002) and (211) reflection of apatite phase accordingly [42]. The characteristic reflections of hydroxyapatite have been identified clearer for the sample soaked for 20 days.
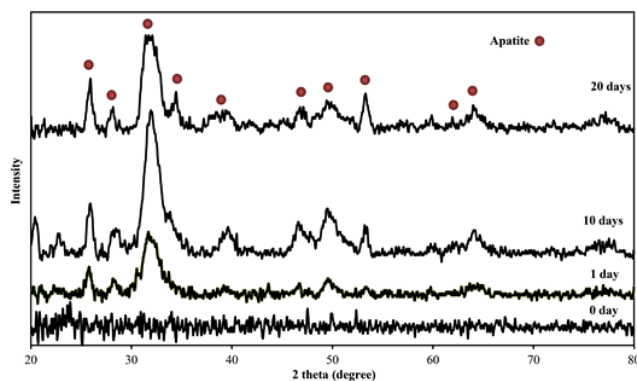

Fig. 8. The XRD pattern of sample BGS after soaking in SBF.

Fig. 9 illustrates the FTIR spectra of sample BGS during soaking in SBF at different time intervals. After a day of immersion of sample BGS in SBF, at 564 and 603 cm^{-1} the bending mode of v4(P-O-P) band and at 1260 cm^{-1} the P-O asymmetric stretching vibration of PO$_4^{3-}$ in apatite was observed. Furthermore, at first day of soaking in SBF a broad pick was observed at 1500 cm^{-1} which converts to two separate picks after 20 days of soaking. In a similar study, Mačković considered this pick as adsorbed carbonates on surface v3(CO$_3^{2-}$) [35]. The silica vibrations, Si-O-Si bending, Si-O-Si symmetric stretching and Si-O-Si asymmetric stretching modes are noticed at 464, 800 and 1088 cm^{-1}, respectively. In addition, the absorption band at

3430 and 1636 cm^{-1} were assigned to OH. The FTIR results in agreement with XRD results confirms the formation of apatite just after one-day soaking of the sample BGS in SBF [53,54].
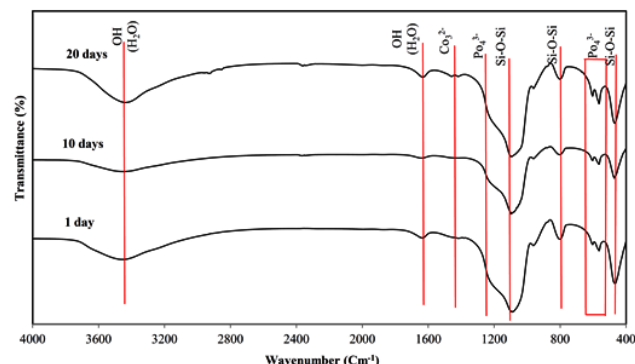

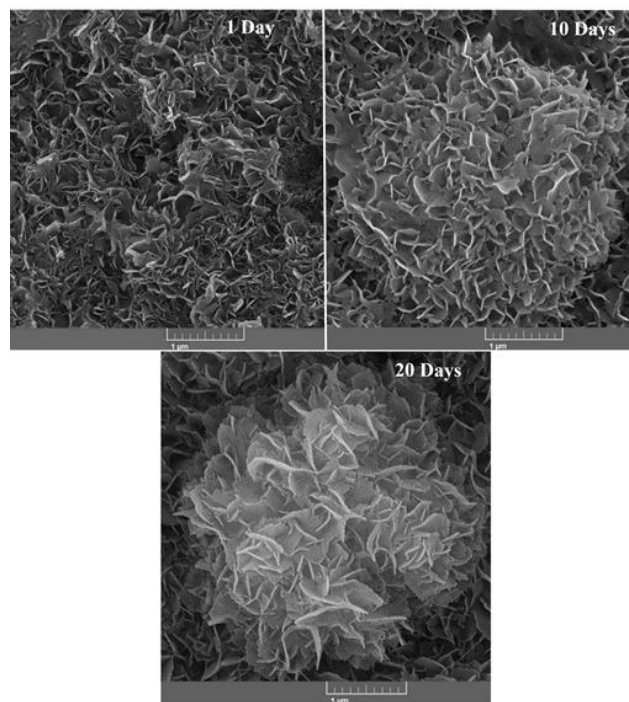**Fig. 9.** FTIR spectra of BGS during soaking in SBF.

Fig. 10. FE-SEM images of sample BGS after soaking in SBF.

The FE-SEM images of BGS sample after soaking in SBF in different periods of time are displayed in **Fig. 10**. The SEM images also indicated the formation of hydroxyapatite on the surface of BGS after the first day of soaking. After 10 days, plate-like crystals were found to be more visible on the surface of BGS. Finally, flowers-like microspheres with diameters about 2 μm self-assembled from growth of plate-like crystals on the surface of BGS [36]. The evaluation of SEM images in different time intervals indicates that the hydroxyapatite is formed at the first day on the surface of BGS but grown at longer times. Similar studies show the formation of hydroxyapatite phase required at least soaking time of 2 days [13]. Letaief et al., reported that porosity on the surface of glass allows a fast nucleation and therefore rapid apatite growth on its surface.

Advanced Materials Letters
www.vbripress.com/aml

IAAM®
Advancement of Materials
to Global Excellence

www.iaamonline.com

So, the main factor contributes the crystallization rate of apatite phase on the surface of glass is textural properties [13]. The formation of hydroxyapatite just one day after soaking of the sample in SBF confirms the high specific surface area of BGS plays an important role in the rate of hydroxyapatite formation.

EDS results of both un-soaked and soaked BGS are shown in **Fig. 11**. The elemental analysis results show, soaking of BGS in the SBF led to a considerable increase in Ca and P elements and a sharp decrease in Si element, which are consistent with the formation of hydroxyapatite in Bioglass [37].
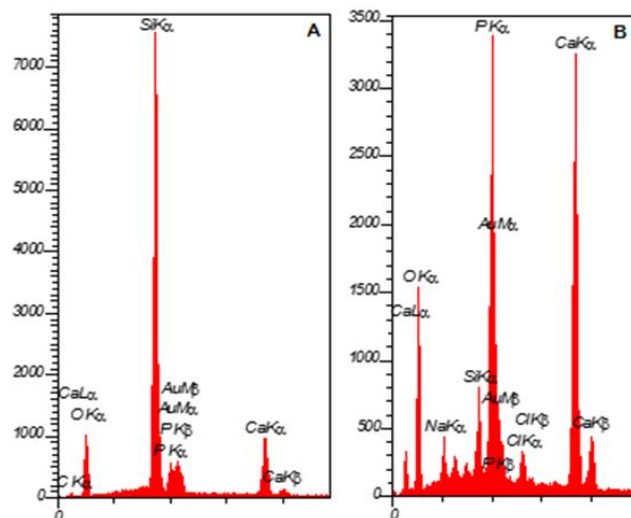

Fig. 11. EDS results of sample BGS before (A) and after (B) soaking in SBF.

Conclusion

Three mesoporous bioactive glasses were synthesized by using two surfactants, SDS as anionic and Triton X-100 as nonionic surfactant by sol-gel method. All three samples present mesoporous structure as a consequence of sol-gel method. Based on results gained in pervious sections, using anionic surfactant is more effective than nonionic surfactant on increasing surface area. In vitro behavior analysis showed that synthesized glasses have ability to form apatite layer on their surface. After only a day fluting in SBF, apatite layer appears on the surface of sample BGS which confirm its bioactivity.

References

1. Arcos, D.; Vallet-Regí, M.; *Acta Biomaterialia,* **2010**, *6,* 2874.
2. Misra, S.K., et al., *Journal of The Royal Society Interface,* **2009**, rsif20090255.
3. Chen, Q.Z.; Thompson, I.D.; Boccaccini, A.R.; *Biomaterials,* **2006**, *27,* 2414.
4. Hench, L.L.; Wilson, J.; *Science,* **1984**, *226,* 630.
5. Jones, J.R.; et al., *Biomaterials,* **2007**, *28,* 1653.
6. Fu, Q.; et al., *Materials Science and Engineering: C,* **2011**, *31,* 1245.
7. Cannillo, V.; et al., *Ceramics International,* **2009**, *35,* 2853.
8. Oliveira, J.; Correia, R.; Fernandes, M.; *Biomaterials,* **2002**, *23,* 371.
9. Oonishi, H.; et al., *Journal of Biomedical Materials Research,* **2000**, *51,* 37.
10. Hench, L.L.; Andersson, O.; *Advanced Series in Ceramics,* **1993**, *1,* 41.
11. Lázaro, G.S.; et al., *Journal of Non-Crystalline Solids,* **2014**, *386,* 19.
12. Li, R.; Clark, A.; Hench, L.; *Journal of Applied Biomaterials,* **1991**, *2,* 231.
13. Balas, F.; Pérez-Pariente, J.; Vallet-Regí, M.; Relationship between bioactivity and textural parameters in glasses in Bioceramics-Conference, **1998**.
14. Ogino, M.; Ohuchi, F.; Hench, L.L.; *Journal of Biomedical Materials Research Part A,* **1980**, *14,* 55.
15. Wu, C.; Chang, J.; *Interface Focus,* **2012**, rsfs20110121.
16. Arcos, D.; et al., *Chemistry of Materials,* **2009**, *21,* 1000.
17. Manzano, M.; Vallet-Regí, M.; *Journal of Materials Chemistry,* **2010**, *20,* 5593.
18. Vallet-Regí, M.; Balas, F.; Arcos, D.; Mesoporous materials for drug delivery. Angewandte Chemie International Edition, **2007**, *46(40),* p. 7548-7558.
19. Vallet-Regí, M.; et al., *Journal of Materials Chemistry,* **2006**, *16,* 26.
20. Mitsuda, K.; Kimura, H.; Murahashi, T.; *Journal of Materials Science,* **1989**, *24,* 413.
21. Ramimoghadam, D.; Hussein, M.Z.B.; Taufiq-Yap, Y.H.; *International Journal of Molecular Sciences,* **2012**, *13,* 13275.
22. Frajkorová, F.; et al., *Ceramics International,* **2015**, *41,* 9770.
23. Sing, K.S.; *Pure and Applied Chemistry,* **1985**, *57,* 603.
24. Gubbins, K.E.; Hysteresis Phenomena in Mesoporous Materials. **2009**.
25. Lowell, S.; et al., Characterization of porous solids and powders: surface area, pore size and density. Vol. 16. **2012**: Springer Science & Business Media.
26. Mitsuda, K.; Kimura, H.; Murahashi, T.; *Journal of Materials Science,* **1989**, *24,* 413.
27. Ramimoghadam, D.; Hussein, M.Z.B.; Taufiq-Yap, Y.H.; *International Journal of Molecular Sciences,* **2012**, *13,* 13275.
28. Frajkorová, F.; et al., *Ceramics International,* **2015**, 41, 9770.
29. Sing, K.S.; *Pure and Applied Chemistry,* **1985**, *57,* 603.
30. Gubbins, K.E.; Hysteresis Phenomena in Mesoporous Materials. **2009**.
31. Lowell, S.; et al., Characterization of porous solids and powders: surface area, pore size and density. Vol. 16. **2012**: Springer Science & Business Media.
32. ElBatal, H. A.; et al. *Materials Chemistry and Physics,* **2003**, *80,* 599.
33. Hench, L. L.; Wilson, J.; *Biomaterials,* **1984**, *5,* 11.
34. Holland L.; The properties of glass surfaces. New York: John, Wiley & Sons, **1964**, p142.
35. Mačković, M.; et al. *Journal of Nanoparticle Research,* **2012**, *14,* 966.
36. Xu, Z.; et al., *RSC Advances,* **2016**, *6,* 76426.
37. Ramimoghadam, D.; Hussein, M.Z.B.; Taufiq-Yap, Y.H.; *International Journal of Molecular Sciences,* **2012**, *13,* 13275.
38. Prabhu, M.; et al. *BioMed Research International,* **2014**, 2014.
39. Stanley, R.; Samson Nesaraj, A.; *International Journal of Applied Science and Engineering,* **2014**, *12,* 9.
40. Singho, Noorsaiyyidah Darman; Rafie Johan, Mohd; *Int. J. Electrochem. Sci.,* **2012**, *7,* 5604.
41. Gorji, B.; et al. *Journal of Applied Chemical Research,* **2012**, *6,* 22.
42. Letaïef, Nouha, et al. *Microporous and Mesoporous Materials,* 2014, *195,* 102.
43. Zana, Raoul et al. *Langmuir,* **1999**, *15,* 2603.
44. Tabia, Zakaria, et al. *RSC Advances,* **2019**, *9,* 12232.
45. López-Noriega, A.; et al. *Chemistry of Materials,* **2006**, *18,* 3137.
46. Cerruti; Marta; David Greenspan; Kevin Powers. *Biomaterials,* **2005**, *26,* 1665.
47. Huo, Qisheng, et al. *Chemistry of Materials,* **1994**, 6, 1176.
48. Wan, Ying, Dongyuan Zhao; *Chemical Reviews,* **2007**, *107,* 2860.

49. Iler, R. K.; "The Chemistry of Silica: solubility, polymerization, colloid and surface and surface properties, and biochemistry." **1979**, 867.

50. Han, Lu; Shunai Che.; *Chemical Society Reviews,* **2013**, *42,* 3740.

51. Arcos, D.; Greenspan, D. C.; Vallet-Regí, M.; *Journal of Biomedical Materials Research Part A: An Official Journal of The Society for Biomaterials, The Japanese Society for Biomaterials, and The Australian Society for Biomaterials and the Korean Society for Biomaterials,* **2003**, *65,* 344.

52. Gerhardt; Lutz-Christian; Aldo R. Boccaccini; *Materials,* **2010**, *3,* 3867.

53. Notingher, I.; Jones, J. R.; Verrier, S.; Bisson, I.; Embanga, P.; Edwards, P.; Polak, J. M.; Hench, L. L.; *Journal of Spectroscopy,* **2003**, *17,* 275.

54. Adams, Luqman A.; Enobong R. Essien; Rafiu O. Shaibu; Aderemi Oki; *New Journal of Glass and Ceramics,* **2013**, *3,* 11.

55. Kumar, Balmiki; Kulanthaivel, Senthilguru; Mondal, Animesh; Mishra, Smruti; Banerjee, Biplab; Bhaumik, Asim; Banerjee, Indranil; Giri, Supratim; *Colloids and Surfaces B: Biointerfaces*, **2017**, 150, 352.

56. Das, Swapan K.; Bhunia, Manas K.; Chakraborty, Debrup; Rahman Khuda-Bukhsh, Anisur; Bhaumik, Asim; *Chemical Communications,* **2012**, *48,* 2891.